MODELLING CRYSTAL MISALIGNMENTS FOR THE X-RAY FEL OSCILLATOR*

R. R. Lindberg[†], Argonne National Laboratory, Lemont, IL 60439 USA

Abstract

The X-ray FEL oscillator has the potential to be a revolutionary new light source providing unprecedented stability in a narrow bandwidth [1]. However, a detailed understanding of cavity tolerance and stability has only begun, and there are presently no suitable simulation tools. To address this issue, we have developed a fast FEL oscillator code that discretizes the field using a Gauss-Hermite mode expansion of the oscillator cavity. Errors in crystal alignment result in a mixing of the modes that is easily modeled with a loss and coupling matrix. We show first results from our code, including the effects of static and time-varying crystal misalignments.

INTRODUCTION

The x-ray FEL oscillator [1, 2], in which the output from a low-gain FEL is returned to interact with subsequent electron bunches by an x-ray cavity built of Bragg crystals and focusing elements, has garnered much interest over the past decade. In this paper we will focus on how the output of a single frequency component can be affected by crystal tilts, as this will provide the first look into what tolerances we require for the crystal optics.

XFELO CAVITY MODES

We expand the transverse profile using the Gauss-Hermite modes defined by the optical cavity. Along x we write

$$
\begin{aligned}
E(x;z) &= \sum_\ell \frac{\mathcal{E}_\ell(z) \exp\left[-\frac{x^2(1+iz/z_R)}{4\sigma_x^2(1+z^2/z_R^2)}\right]}{\sqrt{2^\ell \ell!}\, \sigma_x (1+z^2/z_R^2)^{1/2}} \\
&\quad \times H_\ell\left[\frac{x/\sigma_x}{\sqrt{2(1+z^2/z_R^2)}}\right] e^{-i(\ell+1/2)\mathrm{atan}(z/z_R)} \quad (1)\\
&= \sum_\ell \mathcal{E}_\ell(z) M_\ell(x;z), \quad (2)
\end{aligned}
$$

where M_ℓ is the mode shape of the ℓth Gauss-Hermite mode that is defined in terms of the rms width σ_x and the Rayleigh range $z_R = \sigma_x/\sigma_{x'} = 2k_1\sigma_x^2$ for a paraxial field with carrier wavevector $k_1 = 2\pi/\lambda_1$; a similar expansion holds in y. Ignoring slippage, the FEL field equation is then

$$
\frac{d}{dz}\mathcal{E}_{\ell,m} = -\frac{ek_1 K[\text{JJ}]}{4\gamma_0\epsilon_0} \sum_j e^{-i\theta_j} M_\ell(x_j)M_m(y_j), \quad (3)
$$

where the sum is over all particles in the FEL slice, γ_0 is the reference energy, the ponderomotive phase $\theta_j(z) = (k_1 + k_u)z - ck_1 t_j(z)$ for a particle with time t_j moving in an electromagnetic wave with wavenumber $k_1 = 2\pi/\lambda_1$ and undulator wavenumber $k_u = 2\pi/\lambda_u$, e and ε_0 are the electric charge and permittivity of free space, and [JJ] is the Bessel function factor for an undulator with deflection parameter K. The equations of motion for the phase θ_j and the scaled particle energy difference $\eta_j = (\gamma_j - \gamma_0)/\gamma_0$ are

$$
\frac{d\theta_j}{dz} = 2k_u\eta_j - \frac{k_1}{2}(\boldsymbol{p}_j^2 + K^2 k_u^2 \boldsymbol{x}_j^2/2\gamma^2) \quad (4)
$$

$$
\frac{d\eta_j}{dz} = \frac{eK[\text{JJ}]}{2mc^2\gamma_0^2} \sum_{\ell,m} \mathcal{E}_{\ell,m} e^{i\theta_j} M_\ell(x_j)M_m(y_j) + c.c., \quad (5)
$$

where transverse position and angle are $\boldsymbol{x}_j$ and $\boldsymbol{x}'_j$.

Upon exiting the undulator, the field is returned to the undulator beginning by the x-ray cavity. For a perfectly aligned cavity this results in some loss for each mode $\mathcal{E}_\ell$, but imperfections and misalignments result in mode coupling and effective loss in the fundamental Gaussian mode.

At lowest order misalignments act to shift the optical axis by a position and angle at each pass that can be found by tracking a ray through the system. The result is that the optical axis becomes offset in position by $\boldsymbol{X}_d = (X_d, Y_d)$, and in angle by $\boldsymbol{\Theta}_d = (\theta, \psi)$. Then, the displaced field at the beginning of the undulator for pass $n + 1$ is related to the field at the end of the undulator from pass n via

$$
\begin{aligned}
E^{(n+1)}(\boldsymbol{x};0) &= (1-\alpha)e^{ik(\boldsymbol{x}-\boldsymbol{X}_d)\cdot\boldsymbol{\Theta}_d} \\
&\quad \times E^{(n)}(\boldsymbol{x} - \boldsymbol{X}_d; L_u),
\end{aligned} \quad (6)
$$

where α is the amplitude loss due to imperfect reflectivity. To transform this into a relationship between mode expansion coefficients, we need to project the displaced field onto the Gauss-Hermite basis. We will do this explicitly for the x-direction only, as expressions for y are essentially the same. We insert the expansion (1)-(2), multiply by the mode $M_\ell(x)$, and integrate over x to obtain

$$
\begin{aligned}
\mathcal{E}_\ell^{(n+1)}(0) &= (1-\alpha)\int dx\, e^{ik\theta(x-X_d)} M_\ell(x) \\
&\quad \times \sum_{\ell'} M_{\ell'}(x-X_d)\mathcal{E}_{\ell'}^{(n)}(L_u). \quad (7)\\
&= (1-\alpha)\sum_{\ell'} \mathcal{P}_{\ell,\ell'}(\theta, X_d)\mathcal{E}_{\ell'}^{(n)}(L_u), \quad (8)
\end{aligned}
$$

where we have defined the projection operator $\mathcal{P}$ as shown. It turns out that this integral can be done in terms of the associated Laguerre polynominal $L_n^m(x)$; if $\ell \geq \ell'$ we have

$$
\begin{aligned}
\mathcal{P}_{\ell,\ell'} &= \sqrt{\ell'!/\ell!}\, e^{-ik_1 X_d\theta/2} e^{-[(X_d/\sigma_x)^2+(\theta/\sigma_{x'})^2]/8} \\
&\quad \times \left(\frac{X_d + iz_R\theta}{\sqrt{2}\sigma_x}\right)^{\ell-\ell'} L_{\ell'}^{\ell-\ell'}\left(\frac{X_d^2 + z_R^2\theta^2}{4\sigma_x^2}\right), \quad (9)
\end{aligned}
$$

Table 1: XFELO Parameters for Simulations

Name	Symbol	Value
Energy	$\gamma_0 mc^2$	7 GeV
Energy spread	σ_γ/γ_0	2×10^{-4}
Normalized emittance	ε_n	$0.2\text{mm} \cdot \text{mrad}$
Peak current	I	10 A
Undulator periods	N_u	3000
Undulator length	L_u	53 m
Rayleigh range	Z_R	10 m

while the expression for $\ell' > \ell$ can be obtained by exchanging ℓ and ℓ' and setting $X_d \rightarrow -X_d$ in the second line of (9). The code consists of solving the FEL equations (3)-(5), followed by applying the cavity misalignment operation (8) with $\mathcal{P}$ defined in (9).

RESULTS

The FEL gain can be represented as a matrix $\mathcal{G}$ that joins the field coefficient $\mathcal{E}_\ell^{(n)}(0)$ at the beginning of the nth pass to that at the end of the undulator in the following manner:

$$\mathcal{E}_\ell^{(n)}(L_u) = \sum_{\ell'} \mathcal{G}_{\ell,\ell'} \mathcal{E}_{\ell'}^{(n)}(0). \qquad (10)$$

In the linear gain regime $\mathcal{G}$ is independent of $\mathcal{E}$, while in general it is found by solving the FEL equations (3)-(5). Our first test of the code was to compare the the gain matrix with that of the theory in [3]. The test example assumed an XFELO with nominal gain $\mathcal{G}_{00} \approx 0.184 + 0.075i$, and we found agreement to better than 10% for both the real and imaginary parts of the $5{\times}5$ submatrix joining the five lowest order Gauss-Hermite modes. To go further, we write out the complete mapping from pass to pass as

$$\mathcal{E}^{(n+1)} = (1 - \alpha)\mathcal{P}(\Theta_d, X_d)(\mathbb{1} + \mathcal{G})\mathcal{E}^{(n)}. \qquad (11)$$

If we subtract $\mathcal{E}^{(n)}$ from both sides and approximate $\mathcal{E}^{(n+1)} - \mathcal{E}^{(n)} \approx d\mathcal{E}^{(n)}/dn \rightarrow \Lambda\mathcal{E}$ as is appropriate for a low gain system in the linear gain regime, we can rewrite (11) as the following linear matrix system

$$\Lambda\mathcal{E} = [(1 - \alpha)\mathcal{P}(\Theta_d, X_d)(\mathbb{1} + \mathcal{G}) - \mathbb{1}]\mathcal{E}, \qquad (12)$$

where Λ is a complex growth rate (eigenvalue). We solved this for various optical axis displacements and compared the results to simulations in Fig. 1. For these and the following simulations we use the XFELO parameters suggested in [4] and listed in Table 1, although subsequent work has shown that significantly higher gains can be achieved (see, e.g., [5]); here the nominal power gain $2\Re(G_{00}) \approx 0.36$, the losses $2\alpha = 0.2$, while the displacement $X_d/\sigma_r = 0.1$ corresponds to a crystal tilt of about 20 nrad (the scaled angular offset $\theta/\sigma_{r'} \approx 0.1 X_d/\sigma_r$ is small).

Next, we'll want to look at how misalignments affect saturated output of an XFELO. We begin by considering static misalignments for the same parameters as in Table 1. From

(a)

(b)
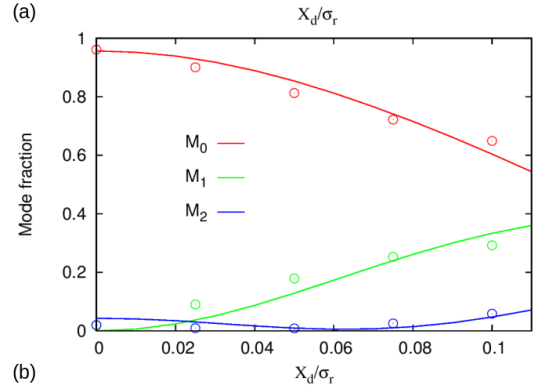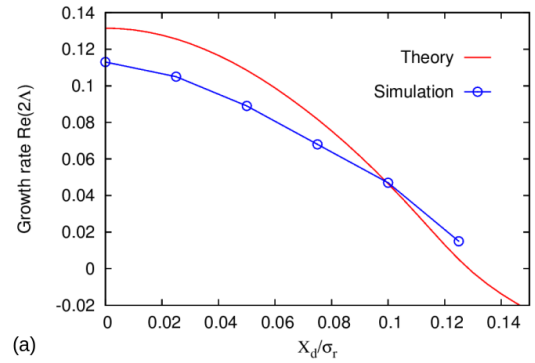
Figure 1: Comparison of theory (solid lines) and simulation (points) for the growth rate (a) and mode content (b) of an XFELO that has a static misalignment leading to a displaced optical axis of X_d/σ_r. Parameters are from Table 1.

Fig. 1 we find that the gain will vanish and the output will be near zero when the crystal misalignments result in a displacement $X_d \approx 0.15\sigma_r$. Thus, we chose $0 \leq X_d \leq 0.1\sigma_r$, which roughly corresponds to varying the crystal misalignment between 0 and 20 nrad. We plot the results of the static misalignment in Fig. 2(a). We find that as the net linear gain 2Λ decreases from about 0.12 for perfect alignment to 0.04 when $X_d = 0.1\sigma_r$, the output power reduces from 1.2 MW to $\sim .23$ MW. Note that at the low end only about 62% of this power is contained in the Gaussian mode, while $\sim 30\%$ is in antisymmetric modes.

In practice the crystal tilts will vary with time. From general physical principles we expect variations that are much slower than the cavity ring-down time will directly imprint themselves upon the output, while fluctuations that occur over much faster time-scales will be averaged over; in other words, in the former case the output power will vary as a function of time such that its value matches that predicted by the steady-state results in Fig. 1, while in the latter case the output should be relatively constant but at a somewhat lower value. We plot results from these two extreme cases in Fig. 2(b) and (c). Panel (b) plots the power as a function of pass number when the crystal tilt oscillates with a period $T = 400$, which is much longer than 2π times the ring-down time $2\pi/\alpha \sim 60$. In this case the output power is approximately given by

$$P_{\text{out}} \approx P_{\text{ideal}} \cos^2(2\pi n/T) + P_{X_d} \sin^2(2\pi n/T), \qquad (13)$$

TUP027
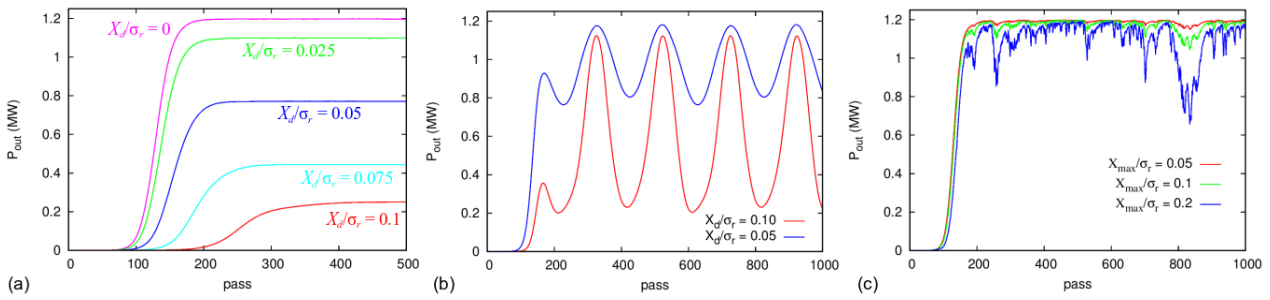
Figure 2: Power output as a function of pass number for cavity misalignments leading to a displaced optical axis of X_d/σ_r. Panel (a) plots steady-state output for static misalignments, while (b) plots the output for slow variations given by $X_d \cos(2\pi n/T)$ for $T = 400$, for which the output oscillates with half the period $T/2$ and the maxima and minima are roughly defined by the static predictions in panel (a). Panel (c) plots the output for random variations on a pass-to-pass basis, where the same pseudo-random sequence is used but with different maximum amplitudes $X_{\max}$.

and the power oscillates with a period $T/2$ between the value its ideal value P_{ideal} and that with the maximal tilt P_{X_d}.

In the other extreme we can imagine a crystal tilt that fluctuates randomly from pass-to-pass. We show three such cases in Fig. 2(c), where we assign the optical axis displacement at any pass the value $rX_{\max}$, with r a random number between -1 and 1. We see that the rms (maximum) power fluctuations are less than 4% (10%) up to value of $X_d = 0.1\sigma_r$, while even $X_d = 0.2\sigma_r$ produces useful output whose rms variations are $\lesssim 10\%$. The general features of each plot are quite similar (e.g., the dip in power near pass 800) because we chose the same pseudo-random sequence for all cases. Interestingly, the mean output power does not significantly change for the random variations chosen.

Finally, we would like to understand how power fluctuations occuring at a variety of time scales affect the output. As a first step, we consider sinusoidal perturbations that have different periods. This will provide some insight into how fluctuations characterized by a particular power spectrum will degrade performance. We show the results of this first study in Fig. 3. Panel (a) shows the output fluctuations for an optical axis displacement of $X_d \cos(2\pi n/T)$ with $X_d = 0.1\sigma_r$ and various perturbation periods T, while (b) plot the same thing for $X_d = 0.1\sigma_r$. Both cases essentially follow Eq. (13) when the period of variation $T \geq 200 \gg 2\pi/\alpha = 60$. As the period approaches the cavity ring-down, $T = 100$ and 50, but with a smaller amplitude of the oscillation: the maximum output power is less than P_{ideal} and the minimum power is greater than P_{X_d}. Finally, for variations at the fastest scale $T = 20$, which is about one-third the cavity ring-down time, the power variations are quite small; panel (a) shows rms flucuations of 1.3% when $X_d = 0.1\sigma_r$, while the power variations in panel (b) where $X_d = 0.5\sigma_r$ are $\sim 0.4\%$. Both of these results are consistent with the random fluctuations of Fig. 2(c).

CONCLUSIONS

We have developed a code that simulates the FEL oscillator by representing the field as a sum of its cavity modes.
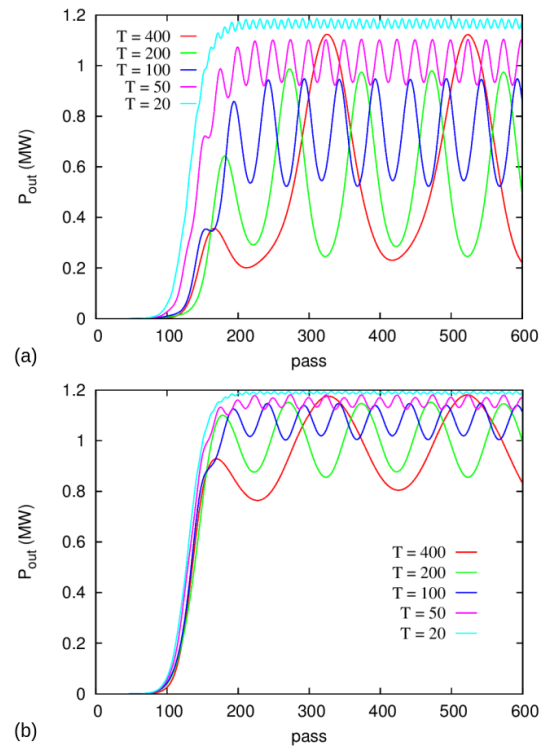
Figure 3: Saturated FEL output for an oscillating optical axis displacement of $X_d \cos(2\pi n/T)$, where $X_d = 0.1\sigma_r$ in panel (a), and $X_d = 0.05\sigma_r$ in panel (b).

When the FEL gain is low the field is well-represented by a few low-order modes, and the code is very efficient. Adding imperfections of the cavity can be done in a straightforward manner, and we have illustrated this by examining how the XFELO output varies with a variety of fluctuating crystal misalignments. The results here have been for a single cavity configuration, and future work will be to do similar tests when the FEL gain is higher, and for cavities that are designed to balance the requirements of FEL gain with the desire to have a system that is more robust to various cavity fluctuations and imperfections.

REFERENCES

[1] K.-J. Kim, Y. Shvyd'ko, and S. Reiche, "A Proposal for an X-Ray FEL Oscillator with an Energy-Recovery Linac," *Phys. Rev. Lett.* **100**, 244802, 2008.

[2] R. Colella and A. Luccio, "Proposal for a free electron laser in the X-ray region," *Opt. Comm.* **50**, 41, 1984.

[3] G.-T. Park, "Performance-limiting factors for x-ray free-electron laser oscillator as a highly coherent, high spectral purity x-ray source," PhD thesis, U. Chicago, 2012.

[4] R. R. Lindberg, K.-J. Kim, Yu. Shvyd'ko, and W. M. Fawley, "Performance of the x-ray free-electron laser oscillator with crystal cavity," *Phys. Rev. ST-AB* **14**, 010701, 2011.

[5] W. Qin, *et al.*, "Start-to-end simulations of for an X-ray FEL oscillatot at the LCLS-II and LCLS-II-HE," in *Proc. FEL 2017*, pp. 247, 2017.